Turkish Journal of Electrical Engineering & Computer Sciences

http://journals.tubitak.gov.tr/elektrik/

Research Article

Turk J Elec Eng & Comp Sci
(2015) 23: 459 – 479

doi:10.3906/elk-1206-114

Improving the performance of primal–dual interior-point method in inverse conductivity problems

Ashkan JAVAHERIAN[1,*], **Amir MOVAFEGHI**[2], **Reza FAGHIHI**[1], **Effat YAHAGHI**[3]

[1]School of Mechanical Engineering, Shiraz University, Shiraz, Iran

[2]Nuclear Safety and Radiological Protection Department, Nuclear Science and Technology Research Institute, Tehran, Iran

[3]Department of Physics, Imam Khomeini International University, Ghazvin, Iran

Received: 27.06.2012 • **Accepted:** 02.04.2013 • **Published Online:** 23.02.2015 • **Printed:** 20.03.2015

Abstract: This study improves the performance of primal–dual interior-point method in inverse conductivity problems via replacing the conventional, complicatedly calculated scalar regularization parameter with a diagonal matrix termed "multi-regularization parameter matrix" here. The solution of the PD–IPM depends considerably on the choice of the regularization parameter. Calculation of the optimal regularization parameter, which yields the most accurate solution, is not simple due to the long iterative nature of the algorithm. The objective optimization, which is implemented by minimizing error in the solutions over an extensive range of the regularization parameters, yields the most accurate solution that can be achieved, although this method is not applicable in reality due to lack of knowledge about the actual conductivity field. However, the modified algorithm not only solves the problem independently using the regularization parameter, but also increases the accuracy of the solution, as well as its sharpness in comparison to the objective optimization.

Key words: Inverse conductivity problem, primal–dual interior-point method, multi-regularization parameter matrix, regularization parameter

1. Introduction

Electrical impedance tomography (EIT) seeks to determine internal conductivity distribution within a medium by successively injecting low amplitude currents and reading the resulting voltages through a number of electrodes attached to the surface of the medium. The calculation of conductivity from the boundary data is a highly ill-posed inverse problem, and must therefore be regularized. Classical smoothness regularization techniques often act as low-pass filters on linearized forward operators in order to dampen higher singular values producing noisy observations [1]. The resulting model is thus spanned by the singular vectors with slow spatial changes. Concisely, quadratic regularization stabilizes the solution at the expense of spatial resolution.

However, total variation (TV) regularization can stabilize the ill-posed problem without imposing any smoothness on the solution. This method thus preserves discontinuities on the reconstructed profiles, producing a sharp transition of conductivity over the intermedium boundaries [2].

Minimization of the TV function was first introduced by Rudin et al. [3] and Dobson and Santosa [4] in the context of image restoration. The solution was iteratively approached based on the steepest descent

*Correspondence: ashkan.javaherian@yahoo.com

method, with time as an evolution parameter and a fixed step size forced to take small value to preserve the solution around the trust region. As a result, the convergence of this algorithm was slow.

To overcome non-differentiability of the absolute TV function at zero, Acar and Vogel [5] and Dobson and Santosa [6] substituted the absolute gradient function $|\nabla f|$ with a polynomial ($\sqrt{|\nabla f|^2+\beta}$). However, this may impose some numerical errors on the solution.

Newton's method was employed by Vogel and Oman [7] and Chan et al. [8,9]. This algorithm is more stable than the steepest descent, but has a small convergence region with respect to β [10]. Chan et al. [8] modified this algorithm so that it is initialized with larger values for β, and continues with decreasing values. Chan et al. [9] applied a line search to the algorithm as well. Vogel and Oman [7] proposed a new algorithm, the so-called lagged diffusivity, which overcame the poor performance of the steepest descent method, as well as the small stability region of Newton's method. The algorithm was primarily formulated as a fixed-point iteration, directly setting the gradient of the objective function to zero. However, it still converges slightly and becomes unstable for the small values of β.

Addressing the problem of minimizing the sum of Euclidean norms based on a technique, the so-called primal–dual interior-point method (PD–IPM) provides a new class of methods for TV regularization [11–12]. Nowadays, the PD–IPM is widely employed in biomedical inverse problems [13,14]. Borsic [1] applied this algorithm to 2D EIT problems, while Graham [15] modified the algorithm so that it could be applied to 3D EIT models. Borsic et al. [16] showed that this algorithm works better than the lagged diffusivity method with regard to both stability and accuracy. This algorithm involves 2 objective functions, the so-called primal (P) and dual (D). The primal function takes greater values than the dual over all feasible points of the dual variables, except for a single point on which the 2 functions take the same value [11,17–19].

The primal variables are initialized by a 1-step quadratic reconstruction controlled by regularization parameter α_L, while α_T is employed to tune the amount of TV regularization for the 2 discussed objective functions with the same value. A challenge for the PD–IPM algorithm is that estimation of the optimal regularization parameter is more complicated than in the classical regularized problems, since the PD–IPM algorithm involves 2 distinct objective functions. The example in the EIDORS website entitled "Total Variation: choice of hyperparameters" is devoted to this difficulty, and shows that the solution is considerably contingent on the choice of the TV regularization parameter α_T, while variations in α_L give rise to smaller changes in the solution [20].

Applying the classical quadratic regularizations, subjective methods such as the "fixed noise figure" proposed by Adler and Guardo [21] or objective methods like the "Best RES" introduced by Graham and Adler [22] are the most efficient methods for optimizing the solution. Blur radius or RES, however, is merely efficient for measuring the spatial resolution of images reconstructed by traditional quadratic regularization techniques [21,23,24], being unable to measure piecewise constant images produced by the TV regularized algorithms. In such cases, calculation of relative error (RE) is more efficient. However, the objective method is time-consuming as well as impracticable in reality due to lack of information about the actual conductivity field. Furthermore, the present study shows that the fixed noise figure method yields solutions that do not adapt for the amount of noise in data, under- or over-regularizing the solution.

This study proposes a straightforward scheme in which the scalar regularization parameter α_T is replaced by a diagonal matrix extracted from the square sensitivity matrix $\mathbf{J}^T\mathbf{J}$. Graham [15] and Javaherian et al. [25] showed that the optimal amount of regularization needed for varied positioning of a contrast moving throughout

the underlying domain is not constant. For example, applying the algorithm to the side contrasts requires a greater amount of regularization to reach the optimized solution in comparison to the central contrasts. In the present study, the square sensitivity matrix is divided into multiple submatrices so that the mean of entries in each of the resulting submatrices is the regularization parameter to be assigned to the region of the domain corresponding to that submatrix. Bera et al. [26] previously proposed a diagonal regularization matrix whose diagonal entries are determined by the maximal values of each of the acquired submatrices. They demonstrated the preference of their method over the identity regularization matrix for a number of regularization parameters through an iterative Gauss–Newton algorithm regularized by the quadratic norm [26]. Javaherian et al. [27] proposed a 2-step smoothness penalty for a 1-step quadratic algorithm, in which the first step shows that the mean of the submatrices rather than the maximum of those suitably moderates the condition number of the Hessian matrix, so that the sensitivity of the solution to the regularization parameter changes is considerably reduced. However, the need for the regularization parameter selection was not removed. Here, a modified variant of the technique is applied to an iterative total variation regularized solver, i.e. the PD–IPM, in a promoted way so that it directly tunes the amounts of regularization needed over the various regions of the domain, without the need for the selection of the scalar regularization parameter.

Applying simulated or experimental data, the images are reconstructed until a specified stopping criterion is satisfied. The amount of regularization in the PD–IPM algorithm is conducted by the MRPM matrix, as well as multiple specified scalar TV regularization parameters, i.e. the value selected in the EIDORS website, the optimal value calculated by objectively minimizing the RE over a wide range of regularization parameters, and the value calculated by the fixed noise figure method ($NF = 1$) (see [15,21,22,28,29]). The objective optimization yields the most accurate solution among all the scalar regularization parameters. Note that the objective optimization and the fixed noise figure methods are quite lengthy, being inefficient for such an iterative algorithm. Furthermore, the objective optimization cannot be applicable in reality since the actual conductivity distribution is unknown. However, the modified algorithm does not need to be optimized, straightforwardly solving the problem. The results clarify that the proposed multi-regularized approach has, surprisingly, increased the accuracy of the reconstructed images as well as their sharpness when compared to all the selected scalar regularization parameters, even those optimistically calculated by the objective optimization.

2. Method

2.1. PD–IPM (standard algorithm)

The PD–IPM algorithm is implemented in the present study as a class of normalized difference algorithms, which are widely applied to EIT applications, owing to their stability with respect to boundary errors. The PD–IPM has been previously employed in EIT by Borsic et al. [16]. Total variation function $TV(\sigma)$ is considered as jumps of conductivity changes over all edges of the finite element mesh. This function is made up in the form:

$$TV(\sigma) = \sum_i |\mathbf{L}_i \sigma|, \tag{1}$$

where $\mathbf{L}$ is a sparse matrix with a size $e \times n$, in which each row corresponds to each edge in the FEM mesh, being formed as $\mathbf{L}_i = [0, \ldots, 0, l_i, 0, \ldots, 0, -l_i, 0 \ldots 0]$. The 2 non-zero entries pertain to the 2 finite elements connected by edge i, noting that l_i is the length of edge i in the mesh.

The 2 objective functions, the so-called primal and dual, are defined as:

$$P(\sigma) = \arg\min_{\sigma} \frac{1}{2} \|\mathbf{J}\sigma - \mathbf{V}\|^2 + \alpha_T \sum_i |\mathbf{L}_i\sigma|, \tag{2}$$

$$D(\sigma) = \max_{\chi:|\chi_i|\leq 1} \min_{\sigma} \frac{1}{2} \|\mathbf{J}\sigma - \mathbf{V}\|^2 + \alpha_T \sum_i \chi_i |\mathbf{L}_i\sigma|, \tag{3}$$

where σ is the vector of the sought-after conductivity changes of the FEM elements with a size $n \times 1$, $\mathbf{V}$ is the normalized measurement data having a size $m \times 1$, $\mathbf{J}$ is the normalized Jacobian matrix with a size $m \times n$, and χ is the vector of bounded scalar dual variables with a size $e \times 1$, which satisfies the following equation for each i.

$$|\mathbf{L}_i\sigma| = \max_{\chi_i:|\chi_i|\leq 1} \chi_i \mathbf{L}_i\sigma. \tag{4}$$

The primal objective function typically takes greater values than the dual function. Exceptionally, the 2 functions take the same value on a single point, which is the optimal point for both primal and dual. Setting the difference between the primal and dual objective functions to zero, the solution of the algorithm will be the joint vectors (σ, χ), which satisfy the 3 conditions:

$$|\chi_i| \leq 1 i = 1, \ldots, e; \tag{5}$$

$$\mathbf{J}^T(\mathbf{J}\alpha - \mathbf{V}) + \alpha_T \mathbf{L}\alpha = 0 \tag{6}$$

$$(|\mathbf{L}_i\sigma| - \chi_i |\mathbf{L}_i\sigma|) = 0 i = 1, \ldots, e. \tag{7}$$

Eq. (5) is feasibility condition, Eq. (6) is first order condition for the inner minimization on σ, and Eq. (7) maintains a condition called "complementarity condition". The non-differentiability of $|L_i\sigma|$ in the neighborhood of zero is addressed by replacing that with $\sqrt{|L_i\sigma|^2 + \beta}$, leading to a smoother condition, the so-called "centering condition".

Applying the Gauss–Newton method yields an iterative algorithm with the following updates at iteration k:

$$\delta\sigma_k = -\left(\mathbf{J}^T\mathbf{J} + \alpha_T \left[\mathbf{L}^T\mathbf{E}_k^{-1}\mathbf{F}_k\mathbf{L}\right]\right)^{-1} \left(\mathbf{J}^T(\mathbf{J}\delta\sigma_k - \mathbf{V}) + \alpha_T \left[\mathbf{L}^T\mathbf{E}_k^{-1}\mathbf{L}\sigma_k\right]\right), \tag{8}$$

$$\delta\chi_k = -\chi_k + \mathbf{E}_k^{-1}\mathbf{L}\sigma_k + \mathbf{E}_k\mathbf{F}_k\mathbf{L}\delta\sigma_k, \tag{9}$$

where

$$\mathbf{E}_k = diag\left(\sqrt{|\mathbf{L}_i\sigma|^2 + \beta}\right), \tag{10}$$

$$\mathbf{F}_k = diag\left(1 - \frac{\chi_i^{(k)}\mathbf{L}_i\sigma_k}{\sqrt{|\mathbf{L}_i\sigma_k|^2 + \beta}}\right). \tag{11}$$

The primal values are initialized by a 1-step quadratic reconstruction conducted by regularization parameter α_L, while the dual values start at zero, the inner point of the bounded region. To update the dual variables in a way in which the dual feasibility condition is retained, Borsic et al. [16] calculated the exact step length to the dual bounds by applying a method proposed by Andersen et al. [12], the so-called step length rule.

The high stability of the algorithm allows its progression with a greater number of iterations. The primal objective function iteratively converges with the progression of the algorithm until the iteration where the following stopping criterion, the convergence condition, is satisfied.

$$\left[\frac{P(\sigma_{k+1})}{P(\sigma_k)} - 1\right] \leq 0.01. \tag{12}$$

2.2. MRPM (modified algorithm)

According to Section 1, estimation of the regularization parameter for the PD–IPM algorithm is more complicated than that of the classical quadratic regularized algorithms. To evade selection of this parameter, the scalar TV regularization parameter (α_T) is replaced by a diagonal matrix, the MRPM. The proposed scheme suitably reduces the condition number of the augmented Hessian matrix $\left(\mathbf{J}^T\mathbf{J} + [\mathbf{MRPM}]\,\mathbf{L}^T\mathbf{E}_k^{-1}\mathbf{F}_k\mathbf{L}\right)$ through the updates of the primal function in a way in which accuracy is retained.

Step 1. The square sensitivity matrix $\mathbf{Z} = \mathbf{J}^T\mathbf{J}$ is calculated, and the diagonal entries are then extracted. Each diagonal entry corresponds to each element in the FEM mesh. The diagonal entries are sorted in ascending order, and the finite elements are mutually numbered according to their values on the diagonal of the square sensitivity matrix.

Step 2. By calculating the new Jacobian matrix ($\mathbf{J}$) around a homogeneous conductivity over the modified FEM mesh, the new square sensitivity matrix Z_{sorted} will again have a size equal to the number of FEM elements. By dividing the square sensitivity matrix of size n into X submatrices of size Y, the FEM mesh made up of n elements is segmented to X distinct subdomains having Y elements as follows:

$$Z_{sorted} = \begin{bmatrix} S_{11} & \cdots & S_{1j} & \cdots & S_{1X} \\ \vdots & \ddots & \vdots & \cdots & \vdots \\ S_{i1} & \cdots & S_{ii} & \cdots & S_{iX} \\ \vdots & \cdots & \vdots & \ddots & \vdots \\ S_{X1} & \cdots & S_{Xj} & \cdots & S_{XX} \end{bmatrix}, \tag{13}$$

where the submatrices are denoted by S_{ij}, and their subscript indicates the location of each submatrix over the square sensitivity matrix. X and Y are often selected such that $n = XY$ and $X - Y$ take the minimum value. In this study, the FEM models are constructed by employing m-file "mk_common_model", available on the EIDORS website [24]. This m-file produces 2D meshes in which the total number of elements is square, so that X and Y are selected such that $X = Y = \sqrt{n}$. This situation fails when the algorithm is applied to 3D FEM models, so the minimal of $X - Y$ is calculated.

Step 3. Each submatrix $[\mathbf{S}_{ij}]_{Y\times Y}$ is replaced by a matrix W_{ij} with equal size, i.e.

$$W_{ij} = \begin{cases} \gamma_{ij}\mathbf{I} & i = j \\ \begin{bmatrix} 0 & \cdots \\ \vdots & 0 \end{bmatrix}_{Y\times Y} & i \neq j \end{cases}, \tag{14}$$

where γ_{ij} is the mean of the entries over the submatrix $\mathbf{S}_{ij}$, and $\mathbf{I}$ is the identity matrix of size Y.

Step 4. The multi-regularization parameter matrix, the so-called MRPM here, is made up of matrices

W_{ij} as follows.

$$\mathbf{MRPM} = \begin{bmatrix} W_{11} & \cdots & 0 & \cdots & 0 \\ \vdots & \ddots & \vdots & \cdots & \vdots \\ 0 & \cdots & W_{ii} & \cdots & 0 \\ \vdots & \cdots & \vdots & \ddots & \vdots \\ 0 & \cdots & 0 & \cdots & W_{XX} \end{bmatrix}. \tag{15}$$

Step 5. The scalar TV regularization parameter (α_T) in Eq. (8) is replaced by the MRPM matrix so that the updates of the primal and dual variables are conducted by the elaborated matrix.

2.3. How does the scheme work?

Suppose that an impulse contrast moves from the center to the boundary of a circular finite element model made up of 1024 elements, and 16 frames of this movement are taken so that finite elements aligning a radius of the model are successively selected to represent an impulse contrast with a conductivity of 0.85 Sm^{-1} for each of the taken frames. To calculate the optimal regularization for each of the frames, a classical quadratic norm regularized algorithm, the maximum a posteriori, is successively applied to the frames over an extensive range of the regularization parameters. This attempt has been objectively implemented based on the Best RES method discussed in Graham and Adler [22] by applying 51 regularization parameters evenly spaced from –5 to 0 on a logarithmic scale. Generally, this method does not regard practical issues such as execution time or efficiency, but focuses merely on accuracy of the optimization. Figure 1 reveals that the calculated optimal regularization parameters are not constant over the entire domain, but depend on the normalized radial positioning of the impulse contrast at each frame. This fact implies that the amount of regularization applied to various regions of the model must not be kept constant. According to Figure 1, the optimal regularization calculated at each frame appreciably increases from the centre to the surface, reflecting the fact that the optimal regularization depends considerably on the sensitivity of the surface data to the selected impulse contrasts. It was shown here that the optimal regularization parameter to be assigned to each subdomain can be extracted directly from the Jacobian (sensitivity) matrix. Accordingly, dividing the square sensitivity matrix having a size equal to the number of finite elements divides the overall domain into multiple subdomains so that different regularization parameters are assigned to those subdomains. The regularization parameter assigned to each region is the mean of entries over the submatrix pertaining to that region.

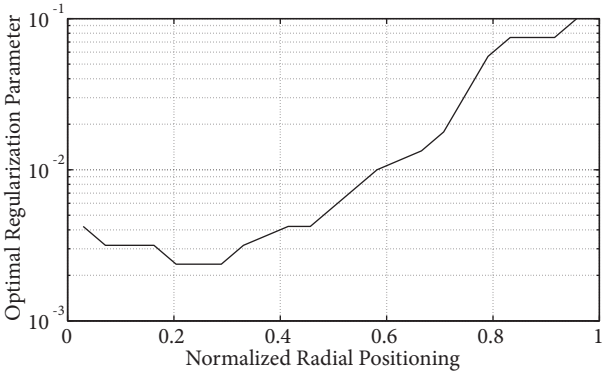

Figure 1. The optimal regularization parameter versus the normalized radial positioning of the impulse inclusion.

3. Results

The PD–IPM algorithm was previously employed in the context of EIT by Borsic et al. [16]. Applying all the simulated and experimental data, the standard algorithm has first been applied as discussed in Section 2.1. The modifications were then exerted on the reconstruction algorithm in order to reconstruct images based on the MRPM scheme discussed in Section 2.2.

3.1. Figures of merits

Relative Error (RE). Applying data for which actual conductivity distribution over the model is known, the accuracy of the reconstructed image is calculated precisely in terms of RE as:

$$RE = \frac{\|\sigma_{reconstructed} - \sigma_{true}\|}{\|\sigma_{true}\|} \times 100\%. \tag{16}$$

Total variation (TV). This measure is the L^1 norm of the conductivity change jumps over the whole domain. The TV is considered the regularizing term in the primal objective function and is calculated by Eq. (1). This measure was considered a parameter for comparing the different TV algorithms in Borsic et al. [16]. However, the present study shows that the TV function is consistently reduced by increases in the regularization parameter as shown in Figure 2; thus, this measure cannot be robust enough to make a fair comparison between algorithms with different amounts of regularization. Moreover, artifacts occurring over the whole image are falsely taken into account by measuring this criterion. It can, however, properly deal with convergence and stability of iterative TV algorithms.

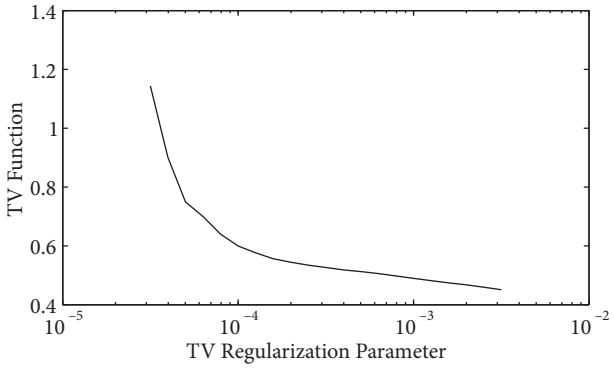

Figure 2. The total variation (TV) as a function of the regularization parameter at the14th iteration of the PD–IPM algorithm applied to the 2D simulated phantom.

Sharpness. The square L^2 norm of conductivity jumps ($\|\mathbf{L}\sigma\|^2$) over the whole of an image will yield a good estimate of the sharpness of that image, if the number of artifacts over the image is not significant. In other words, if the image is sufficiently accurate, the sharpness will be a good measure of discontinuity preservation over the image. For more details, see [16].

3.2. 2D simulated phantom

3.2.1. Forward modeling

The 2D phantom was simulated similarly to those applied by Borsic et al. [16]. The simulated phantom is an FEM mesh made up of 576 triangular elements. The electrodes were defined based on the shunt electrode model

(SEM) for convenience, as this approximation does not affect the comparison between the 2 algorithms [30]. A 16-electrode system was simulated, whereby injecting currents and measuring the corresponding voltages was conducted based on the adjacent drive pattern. The distribution of the conductivity is similar to that defined in Borsic et al. [16], which is a narrow gap between 2 specified more conductive and less conductive regions, thus providing a challenge for the reconstruction. The model has a background conductivity of 1 Sm^{-1}. Borsic et al. [16] provided sharp conductivity jumps on the interdomain interfaces, so the more conductive and less conductive regions had conductivities of 1.5 Sm^{-1} and 0.5 Sm^{-1}, respectively. However, a more difficult situation in which the conductivities of the inclusions are moderated to be 1.1 Sm^{-1} and 0.9 Sm^{-1} was considered in this study in order to show that the proposed scheme has the capability of reconstructing smaller conductivity jumps as well. Note that the TV regularization is typically applicable to piecewise constant conductivity fields having sharp transitions on their interfaces [6,16]. Figure 3 shows the conductivity distribution of the simulated phantom. The noise contributed to the measurement data is an additive white Gaussian noise (AWGN). Considering the difference imaging, which is applied in this study, AWGN is simulated as

$$Noise = NL \times std(\mathbf{V}_2 - \mathbf{V}_1) \times randn, \tag{17}$$

where NL is the noise level, std is standard deviation of difference between 2 frames of data, and randn is pseudorandom values drawn over a standard Gaussian distribution. The data were simulated with 1%, 2%, and 3% noise levels, similar to Borsic et al. [16], as well as 5% in order to appraise the performance of the standard and the modified algorithms over data with high levels of noise.

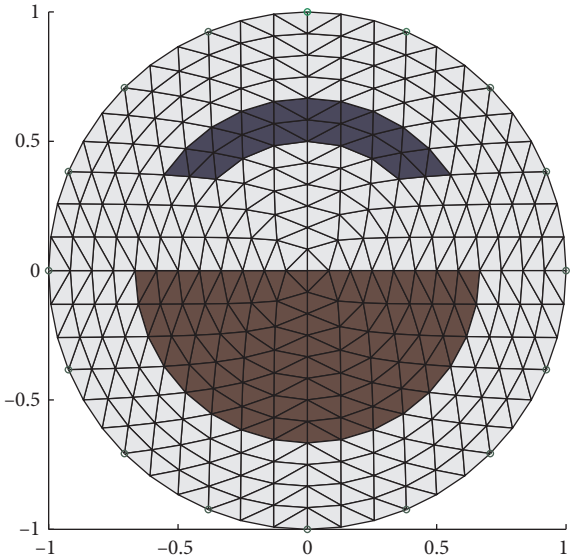

Figure 3. The 2D simulated phantom made up of 576 elements.

3.2.2. Image reconstruction

The images of the simulated phantom were reconstructed on a mesh matching the forward mesh by applying the normalized difference method [15,22]. Employing the standard algorithm, the images have been reconstructed from the simulated noisy data by applying various regularization parameters as follows.

1- Neglecting the less conductive contrast, the 2D model to be imaged is exactly identical to that presented in the EIDORS example entitled "Total Variation reconstruction 2D", and the value applied to this special model

in that example is $\alpha_T = 10^{-3}$ [29]. This value was constantly applied to all the noisy data in the present study. Since the conductivity distribution as well as the noise level affects the amount of required regularization to some extent, this value does not yield the most accurate solution.

2- The optimal value was objectively calculated for each instance of the noisy data as follows. The standard algorithm was successively implemented by a range of the regularization parameter values evenly spaced with a distance of 0.1 on a logarithmic scale ($\alpha_T = logspace(-5, 0, 51)$), and the RE of the reconstructed images at the iteration where Eq. (12) is satisfied, i.e. the 14th iteration, was calculated for each of the selected regularization parameters. Figure 4 shows the RE of the reconstructed images against the applied regularization parameters. Figures 4(a), 4(b), 4(c), and 4(d) pertain to the images reconstructed by the simulated data containing 1%, 2%, 3%, and 5% noise levels, respectively. The optimal regularization parameter is the point that results in the minimum RE over each of these plots. It is clear that the resulting optimal regularization parameters have been suitably adapted for the different amounts of noise levels in the data, producing the most accurate image. Although this method is not applicable in real situations since conductivity distribution of actual models is often unknown, it provides the most accurate solution that can be achieved in simulation, thus making the most optimistic comparison of the standard algorithm to the modified scheme.

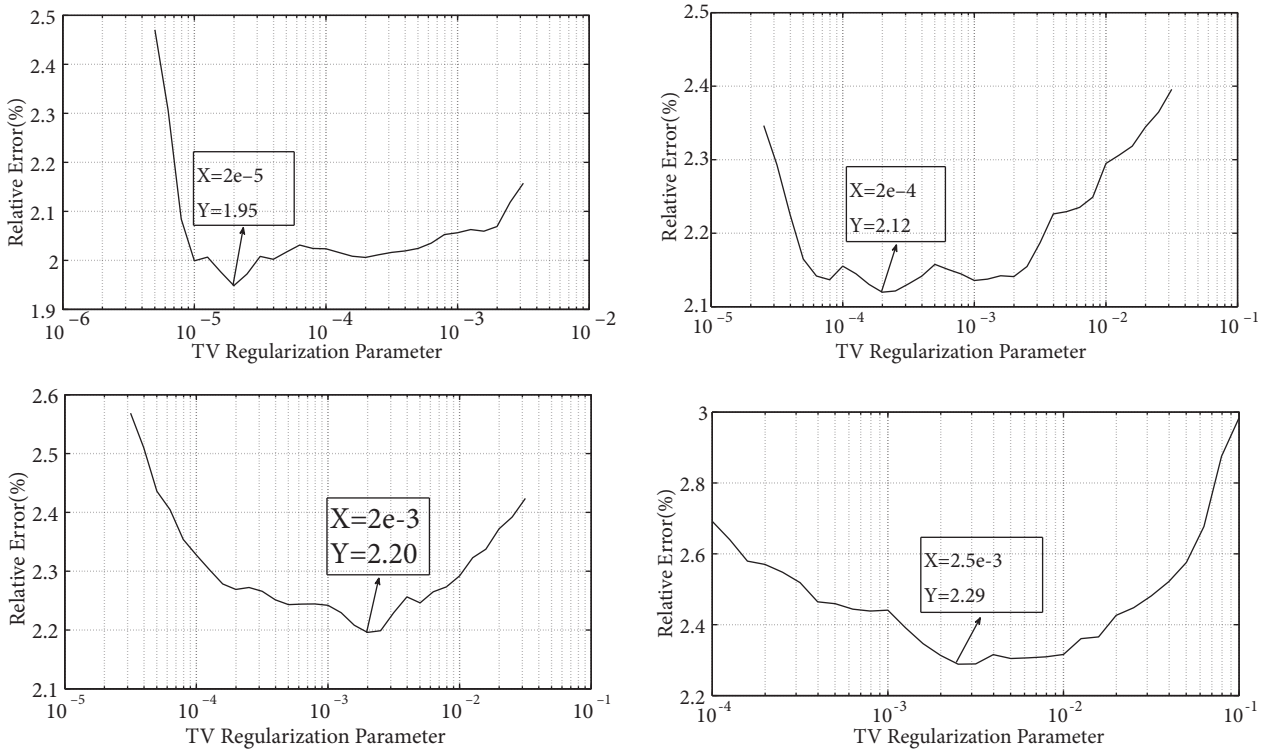

Figure 4. The relative error of the images versus the logarithmic scaled regularization parameter, reconstructed at the 14th iteration of the PD–IPM algorithm. The data have been corrupted with noise levels of (a) 1%, (b) 2%, (c) 3%, and (d) 5%.

3- The third value has been calculated by employing the fixed noise figure method using the EIDORS software. The noise figure is a measure of noise amplification from the data to the reconstructed image; see [21,28] for more details. Graham and Adler [22] showed that the regularization parameter which leads to $NF = 1$ is the best approximation of the optimal regularization. However, this method lacks the ability to

adapt for the different noise levels in data, resulting in a fixed value for all noise levels. The value calculated for the 2D model in the present study is $\alpha_T = 10^{-4}$.

On the other hand, employing the modified scheme, the image has been reconstructed via direct substitution of the scalar regularization parameter by the MRPM matrix, as discussed in Section 2.2.

3.2.3. Observations

Figure 5 shows the images of the 2D phantom, reconstructed at the 14th iteration of the algorithm from the simulated noisy data having a noise level of 3%. Figure 5(a) shows the image reconstructed by the regularization parameter assigned to a similar phantom on the EIDORS website [29]; Figure 5(b) exhibits the optimal image obtained by minimization of the RE values over an extensive range of the regularization parameters; Figure 5(c) has been produced by the fixed noise figure method. However, Figure 5(d), which has resulted from the direct application of the MRPM matrix, yielded the most accurate image. The images reconstructed from the other simulated noisy data have not been shown in this manuscript due to space constraints.

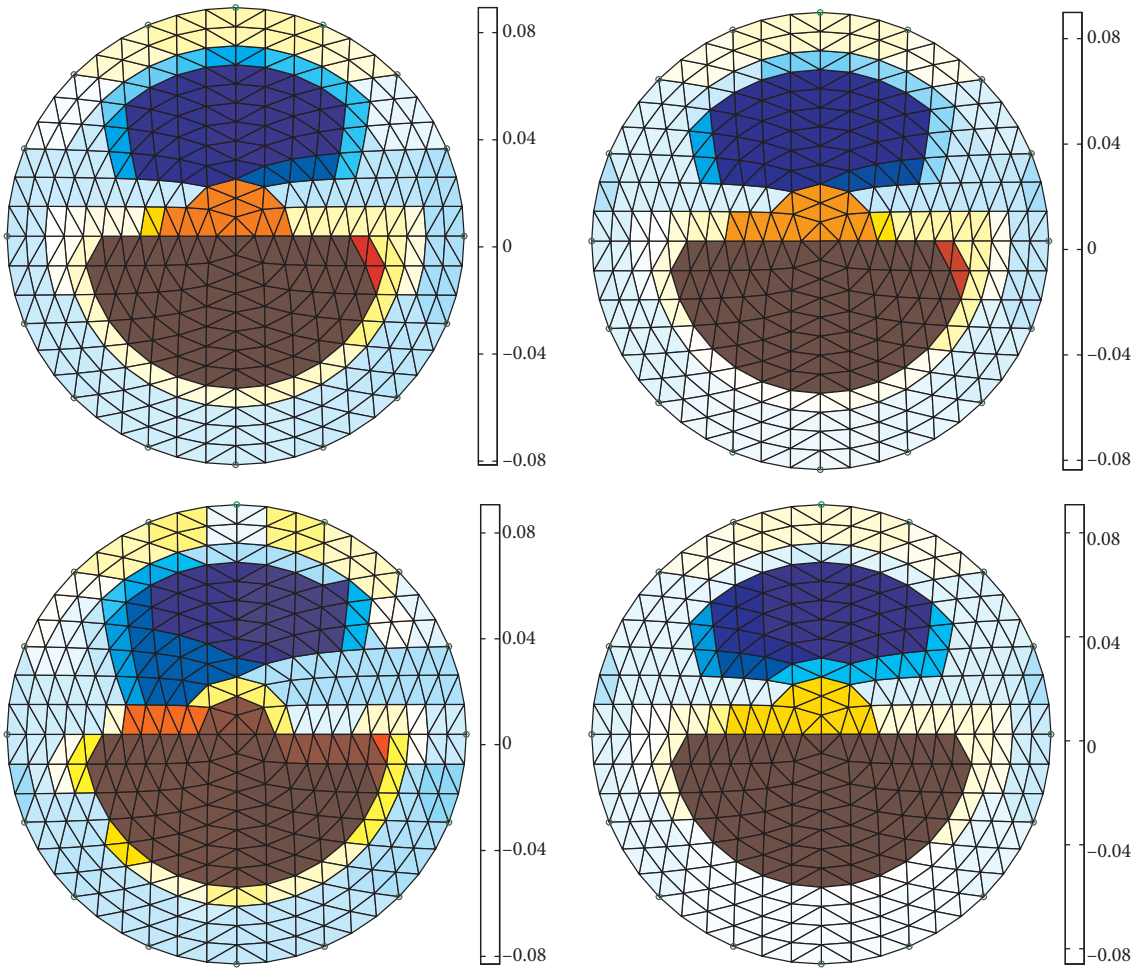

Figure 5. The images of the 2D simulated phantom, reconstructed after the 14th iteration of the PD–IPM algorithm. The data have been simulated with a noise level of 3%. The amounts of regularization are conducted by: (a) EIDORS ($\alpha_T = 10^{-3}$), (b) the objective optimization ($\alpha_T = 2 \times 10^{-3}$), (c) NF=1 ($\alpha_T = 10^{-4}$), and (d) the modified scheme (MRPM matrix).

Figure 6(a) shows the RE of the reconstructed images with the progression of the algorithm for the noisy data simulated with a noise level of 2%. Figure 6(b) exhibits the sharpness of these images in the same way. The green curves relate to the images reconstructed by applying the regularization parameter on the EIDORS site, i.e. $\alpha_T = 10^{-3}$; the blue curves correspond to the regularization parameter calculated by the fixed noise figure method, i.e.$\alpha_T = 10^{-4}$; the red curves pertain to the optimal regularization parameter objectively calculated by the RE minimization. Finally, the black curves have resulted from the images directly reconstructed by applying the MRPM matrix. Figures 7(a) and 7(b) quantify the images reconstructed from the data simulated by a noise level of 3% in the same way as Figures 6(a) and 6(b). Similarly, Figures 8(a) and 8(b) pertain to the images reconstructed from the 5% noisy data. Figure 8(a) clarifies that the fixed noise figure method cannot adapt for the high levels of noise in data, producing images far from true. Accordingly, the blue curve was ignored in Figure 8(b), since the sharpness is merely acceptable as long as accuracy is retained, according to what is discussed in Section 3.1.

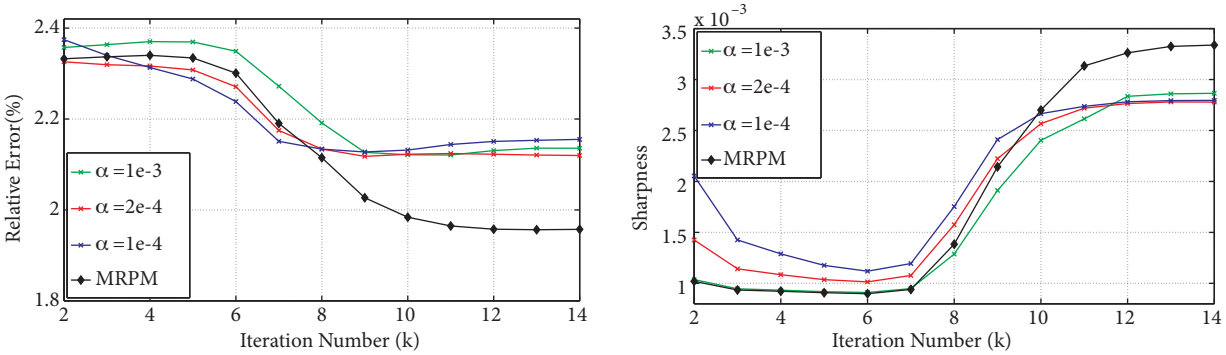

Figure 6. The procedure of the changes in the reconstructed images of the 2D simulated phantom with the progression of the algorithm in terms of: (a) relative error, and (b) sharpness. The data have been simulated with a noise level of 2%.

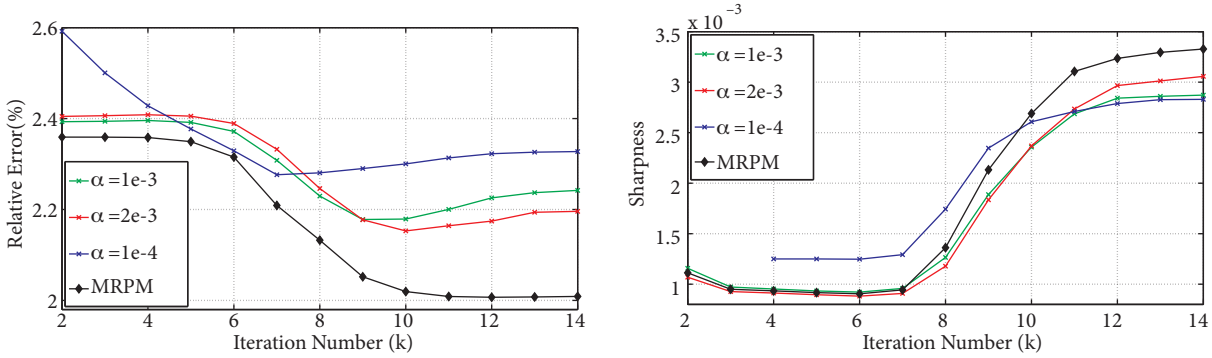

Figure 7. The procedure of the changes in the reconstructed images of the 2D simulated phantom with the progression of the algorithm in terms of: (a) relative error, and (b) sharpness. The data have been simulated with a noise level of 3%.

It must be remembered that the purpose of employing the TV reconstruction algorithms is to reconstruct an image with the highest possible preservation of edges. This is performed via minimizing the L^1 norm of conductivity jumps in a way in which the accuracy does not fail. As shown in Figures 6, 7, and 8, using the standard algorithm, the RE iteratively decreases with the progression of the algorithm through the initial

iterations, but then slightly increases to produce higher sharpness at the expense of accuracy. In other words, the accuracy of the images has degraded in a trade-off with preserving the discontinuities over the simulated domain. This is due to some numerical errors occurring during estimation of the intermedium boundaries. However, by exerting the proposed scheme based on the MRPM matrix, both the sharpness and the accuracy have been consistently improved through all the iterations, and the trade-off has been overridden, so that the interfaces have been reconstructed with much higher accuracy.

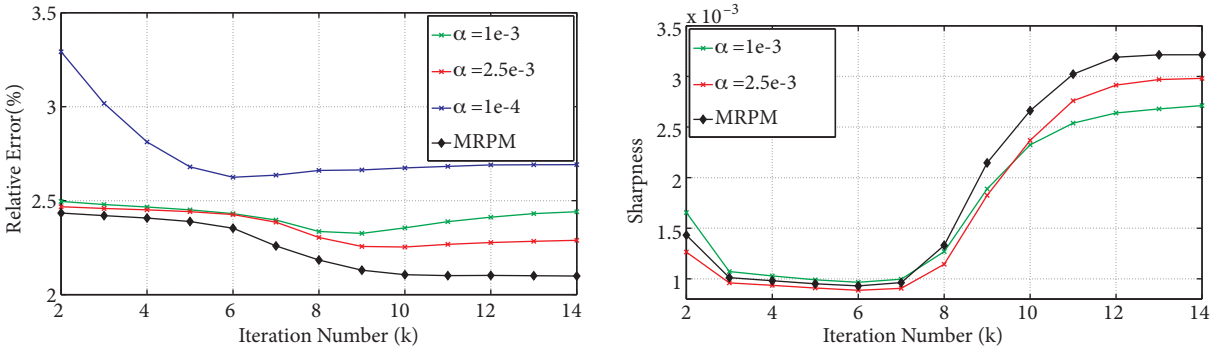

Figure 8. The procedure of the changes in the reconstructed images of the 2D simulated phantom with the progression of the algorithm in terms of: (a) relative error, and (b) sharpness. The data have been simulated with a noise level of 5%.

It can be seen in Figures 6(b), 7(b), and 8(b) that the MRPM scheme enhances the sharpness of the images with the iterative progression of the algorithm as well. Applying the simulated noisy data, the sharpness has been slightly reduced until the 7th iteration, and has then been enhanced abruptly. The fast increases have then been moderated with the convergence of the algorithm until Eq. (12) is satisfied. It is clear that applying the modified algorithm based on the MRPM matrix has given rise to a much higher sharpness, producing a more explicit estimation of discontinuities over the images for all the noisy data, as compared to the standard algorithm using the scalar regularization parameters.

The merits of the standard and the modified algorithms have also been optimistically compared in Table 1, as the objective optimization yields the most accurate solution that can be obtained from applying all the scalar regularization parameters. Note that the objective optimization based on RE minimization is not applicable in reality due to the lack of information about the actual conductivity distribution. According to this table, when applying all the simulated noisy data, the modified algorithm has outperformed the standard algorithm in terms of the RE as well as the sharpness. Note that the modified algorithm is directly implemented by applying the MRPM matrix, whereas the standard algorithm needs to be optimized by employing numerous regularization parameters in order to find the optimal regularization point. The accuracy of the MRPM matrix has even held for much higher levels of noise in data, as will be shown for the 3D simulated phantom.

Table 1. Quantification of the images of the 2D phantom, reconstructed at the 14th iteration of the algorithm.

	Objective optimization					MRPM optimization		
Noise level	α_T	RE (%)	$TV(\sigma)$	$\|\mathbf{L}\sigma\|^2$		RE (%)	$TV(\sigma)$	$\|\mathbf{L}\sigma\|^2$
1%	2e–5	1.95	5.42×10^{-1}	3.43×10^{-3}		1.93	4.68×10^{-1}	3.36×10^{-3}
2%	2e–4	2.12	5.00×10^{-1}	2.78×10^{-3}		1.96	4.68×10^{-1}	3.34×10^{-3}
3%	2e–3	2.20	4.64×10^{-1}	3.06×10^{-3}		2.01	4.68×10^{-1}	3.33×10^{-3}
5%	2.5e–3	2.29	4.60×10^{-1}	2.98×10^{-3}		2.10	4.73×10^{-1}	3.21×10^{-3}

3.3. 3D simulated phantom

3.3.1. Forward modeling

The 3D phantom has been simulated similarly to that presented in the EIDORS example entitled "Compare 3D image reconstruction", as it may be more typical for EIT researchers [31]. The simulated phantom is a cylindrical FEM model, 1 in radius and 3 in height, which is made up of 828 tetrahedral elements. The electrodes were simulated based on the complete electrode model (CEM) so that each of the electrodes was assumed to have an area of 0.196×1, and a contact impedance of 100Ω [30]. The 32 electrodes are equally divided into 2 planes. The placement of the electrodes as well as the measurement protocol was conducted based on the planar strategy discussed in Graham and Adler [32]. The model has a background conductivity of 1 Sm^{-1}. A challenge has been considered so that the conductivities of the contrast regions have been moderated to be 1.1 Sm^{-1} and 0.9 Sm^{-1}, similar to those applied to the 2D phantom, in order to demonstrate that the modified algorithm has the capability to reconstruct smaller conductivity jumps as well. With the exception of this modification, the simulated model is exactly the same as the 3D model shown in the mentioned EIDORS example [31], and is therefore not exhibited in this manuscript due to space constraints. The data were simulated with noise levels of 2%, 3%, 5%, and 10% in order to compare the performance of the standard and the modified algorithms by noisy data with different amounts of noise levels.

3.3.2. Image reconstruction

The images of the simulated phantom were reconstructed on a mesh matching the forward mesh by applying the difference method. Applying each simulated noisy datum, the images have first been reconstructed by applying the standard algorithm optimized via objectively calculating the optimal regularization parameter. The optimal regularization parameter is the point that produces the image with the minimal RE at the 20th iteration of the algorithm, similarly to those applied to the 2D phantom. Note that the convergence condition has been satisfied at the 20th iteration. The regularization parameter applied in the EIDORS example entitled "Compare 3D image reconstruction" [31], and the one calculated by the fixed noise figure, have been ignored since they have given solutions far from the optimal solution.

The modified algorithm has been subsequently employed such that the MRPM matrix was straightforwardly applied to the algorithm in order to adjust the amount of regularization to be applied to various regions of the model.

3.3.3. Observations

Figures 9(a) and 9(b) show the images reconstructed by applying the objective optimization to the data containing 5% and 10% noise levels, respectively. Mutually, Figures 9(c) and 9(d) display the images reconstructed by exerting the MRPM scheme on those data. From these figures, the modified algorithm has produced images with much higher accuracy in comparison to the objective optimization, yielding a more accurate vision of the contrasts. Note that the exact simulated model can be seen in the example titled "Compare 3D image reconstruction" on the EIDORS website [31].

Figure 10(a) shows the procedure of the changes in the RE of the images reconstructed from the data containing a 5% noise level. The red curve corresponds to the images reconstructed by the optimal regularization, while the black curve pertains to the images reconstructed by applying the MRPM matrix. Furthermore, Figure 10(b) shows the sharpness of these reconstructed images in the same way as in Figure 10(a).

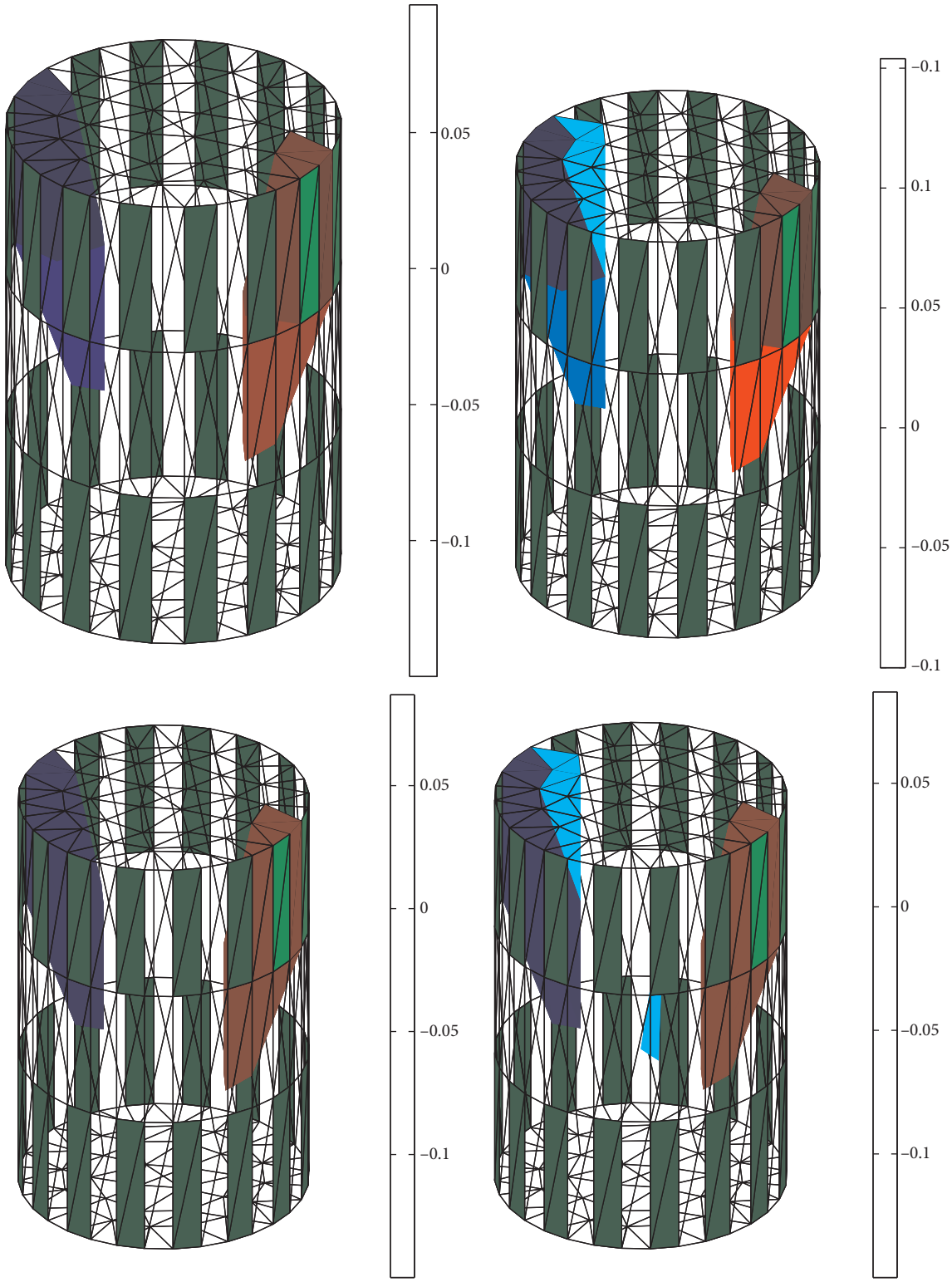

Figure 9. The reconstructed images of the 3D simulated phantom after the 20th iteration of the algorithm, considering: (a) 5% noise level in data, objective optimization; (b) 10% noise level in data, objective optimization; (c) 5% noise level in data, MRPM scheme; (d) 10% noise level in data, MRPM scheme.

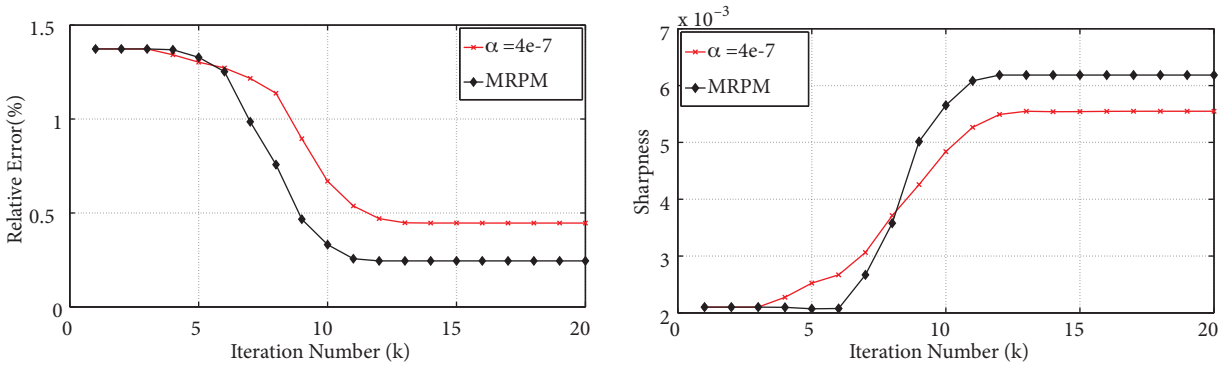

Figure 10. The procedure of the changes in the reconstructed images of the 3D simulated phantom with the progression of the algorithm in terms of: (a) relative error, and (b) sharpness. The data have been simulated with a noise level of 5%.

As shown in these figures, the modified algorithm has successfully improved the RE, as well as the sharpness of the images after expiration of a few initial iterations, compared to the standard algorithm. In applying the other noisy data, the procedure of the changes was similar to that occurring for the noise level of 5%, yielding the values exhibited in Table 2 for the 20th iteration of the algorithm. As shown in this table, the modified scheme has outperformed the standard algorithm in reducing the RE of the reconstructed images, as well as enhancing their sharpness.

Table 2. Quantification of the images of the 3D phantom, reconstructed at the 20th iteration of the algorithm.

Noise	Objective optimization					MRPM optimization		
level	α_T	RE (%)	$TV(\sigma)$	$\|\mathbf{L}\sigma\|^2$		RE (%)	$TV(\sigma)$	$\|\mathbf{L}\sigma\|^2$
2%	1.25e–7	2.22×10^{-1}	4.91×10^{-1}	6.45×10^{-3}		2.20×10^{-1}	4.75×10^{-1}	6.32×10^{-3}
3%	2e–7	2.90×10^{-1}	4.90×10^{-1}	6.18×10^{-3}		2.23×10^{-1}	4.76×10^{-1}	6.29×10^{-3}
5%	4e–7	4.46×10^{-1}	4.84×10^{-1}	5.55×10^{-3}		2.45×10^{-1}	4.87×10^{-1}	6.19×10^{-3}
10%	1e–6	8.65×10^{-1}	4.63×10^{-1}	4.38×10^{-3}		3.74×10^{-1}	5.46×10^{-1}	6.04×10^{-3}

3.4. Experimental results

3.4.1. Golf balls in a pail

A package of experimental data available on the EIDORS website has been considered in order to evaluate the performance of the modified algorithm in comparison with the standard objectively optimized algorithm in experimental applications [33]. This package was created at the University of Ottawa. The phantom is a polyethylene pail, 30 cm in height and diameter, which is filled with 0.9% saline solution. The challenge is to recover images of 2 small nonconductive contrasts. The contrasts are 2 golf balls, 2 cm in radius, which were suspended in the solution. Two setups of this package have been selected. Figure 11 shows the reconstructed images of these setups. Figures 11(a) and 11(b) are the images reconstructed by the objective optimization. Figure 11(a) pertains to the first setup, while the second setup has led to the image presented in Figure 11(b). The positioning of the balls is represented by the red circles. These images have either become magnified or have shifted in comparison to the red circles. Mutually, Figures 11(c) and 11(d) have been reconstructed by applying the MRPM matrix. Unlike the objective optimization, the images reconstructed by applying the MRPM matrix have been approximately matched with the red circles. The merits of the 2 algorithms have been compared in Table 3, in which the reconstructed images after the 15th iteration of the algorithm have been quantified. As

shown in this table, in applying both setups, the modified algorithm has successfully improved the accuracy of the images in terms of the RE as well as the sharpness, compared to the objectively optimized algorithm. In order to calculate the RE in this experiment, σ_{true} in Eq. (16) has been approximated by interpolations in which the finite elements are part of the red circles.

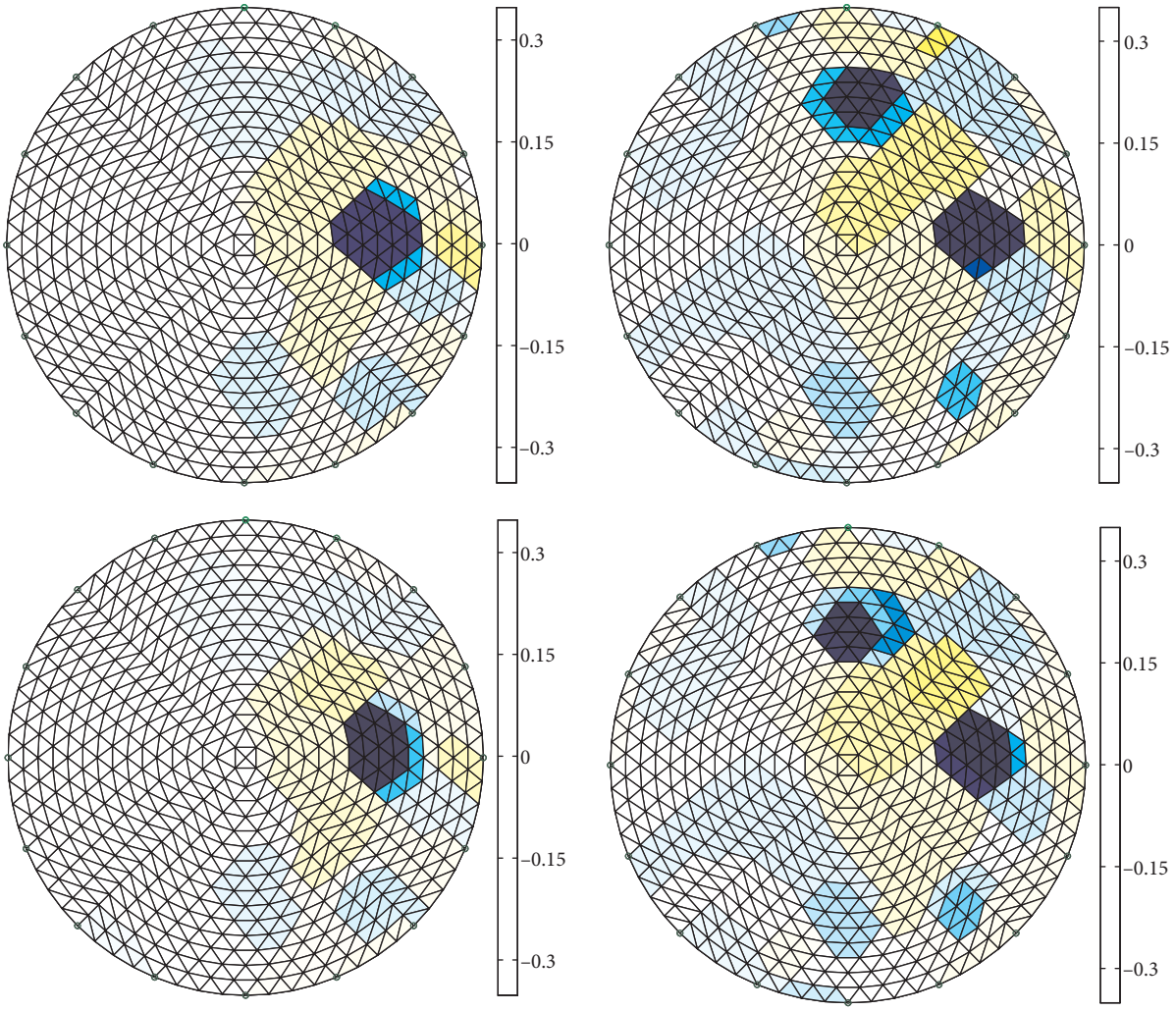

Figure 11. The images of the golf balls, reconstructed after the 15th iteration of the PD–IPM algorithm. The images have been reconstructed by the objective optimization, applying (a) Setup 1: A single ball has been placed in the pail, matching the red circle; (b) Setup 2: Two balls have been placed in the pail, matching the 2 red circles. The images have been reconstructed by the MRPM matrix, applying (c) Setup 1, (d) Setup 2.

Table 3. Quantification of the images of the golf balls, reconstructed at the 15th iteration of the algorithm.

	Objective optimization				MRPM optimization		
Setups	α_T	RE (%)	$TV(\sigma)$	$\|\mathbf{L}\sigma\|^2$	RE (%)	$TV(\sigma)$	$\|\mathbf{L}\sigma\|^2$
One ball	4e–4	4.10	5.45×10^{-1}	7.20×10^{-3}	3.74	5.41×10^{-1}	1.02×10^{-2}
Two balls	4e–4	11.26	1.22	2.23×10^{-2}	5.76	1.19	2.59×10^{-2}

3.4.2. Human lung

At the end of this study, the algorithms were employed in order to reconstruct images of a human lung. The extracted data are available on the EIDORS website for 34 frames of a breathing cycle of a male subject. The data have been embedded in an m-file, namely "montreal_data-1995" [28]. A challenge arose since the actual conductivity distribution of the lung frames was not available. Therefore, the accuracy of the images could not be calculated by the RE introduced in Section 3.1, but was approximately estimated as follows.

Contrast to noise ratio (CNR). Assuming the inhomogeneity area as the one-fourth amplitude set defined by Adler et al. [24], CNR is written as [34,35]:

$$CNR = \frac{|mean_{IR} - mean_{BR}|}{\left(\omega_{IR} SD_{IR}^2 + \omega_{BR} SD_{BR}^2\right)^{1/2}}, \tag{18}$$

where ω_{IR} is the inhomogeneity area divided by the overall image area, ω_{BR} is the background area divided by the overall image area, $mean_{IR}$ and SD_{IR}^2 are respectively the mean and the square standard deviation of finite element conductivities that are within the inhomogeneity area, and $mean_{BR}$ and SD_{BR}^2 are respectively the mean and the square standard deviation of elements within the background area.

Coefficient of contrast (COC). COC is defined as the absolute ratio of the mean contrast conductivity to the mean background conductivity [27], considering the one-fourth amplitude set as the contrast conductivity [24]. COC is written as:

$$COC = \left| \frac{mean_{IR}}{mean_{BR}} \right|. \tag{19}$$

Figure 12 shows the reconstructed images of the 18th and the 22nd frames of the human breathing data available on the EIDORS website. The images have been reconstructed by applying the PD–IPM algorithm to a mesh matching the geometry of the thorax and using the normalized difference method such that the first frame has been employed as the reference measurement. The images were reconstructed at the 12th iteration of the PD–IPM algorithm, where Eq. (12) has been satisfied. Considering Figures 12(a) and 12(b), the amount of regularization has been controlled by the optimal regularization parameter, which results in the maximum value of CNR over a wide range of the scalar regularization parameters ($\alpha_T = 1 \times 10^{-3}$). Figure 12(a) pertains to the 18th frame of data, and Figure 12(b) has been produced from the 22nd frame. The reconstructed images depended considerably on the choices of the regularization parameters, so that regularization parameters smaller than 7×10^{-4} or those greater than 2×10^{-3} falsely produced indistinguishable images.

Replacing the scalar regularization parameter with the MRPM matrix has produced the images shown in Figures 12(c) and 12(d), in which the distortions of the air volume boundary have been moderated in comparison with the best solution of the standard scheme. In other words, the regularization of the algorithm based on the MRPM matrix has successfully provided more explicit estimation of the air volume boundary compared to the objective optimization. The artifacts occurring over the images have been reduced by employing the MRPM matrix as well.

Table 4 shows the quantified values of the images reconstructed at the 12th iteration. The images have been reconstructed from the 18th, 20th, and 22nd frames of the breathing cycle. As shown in this table, the modified scheme has successfully overcome the objective optimization with regard to both the CNR and COC.

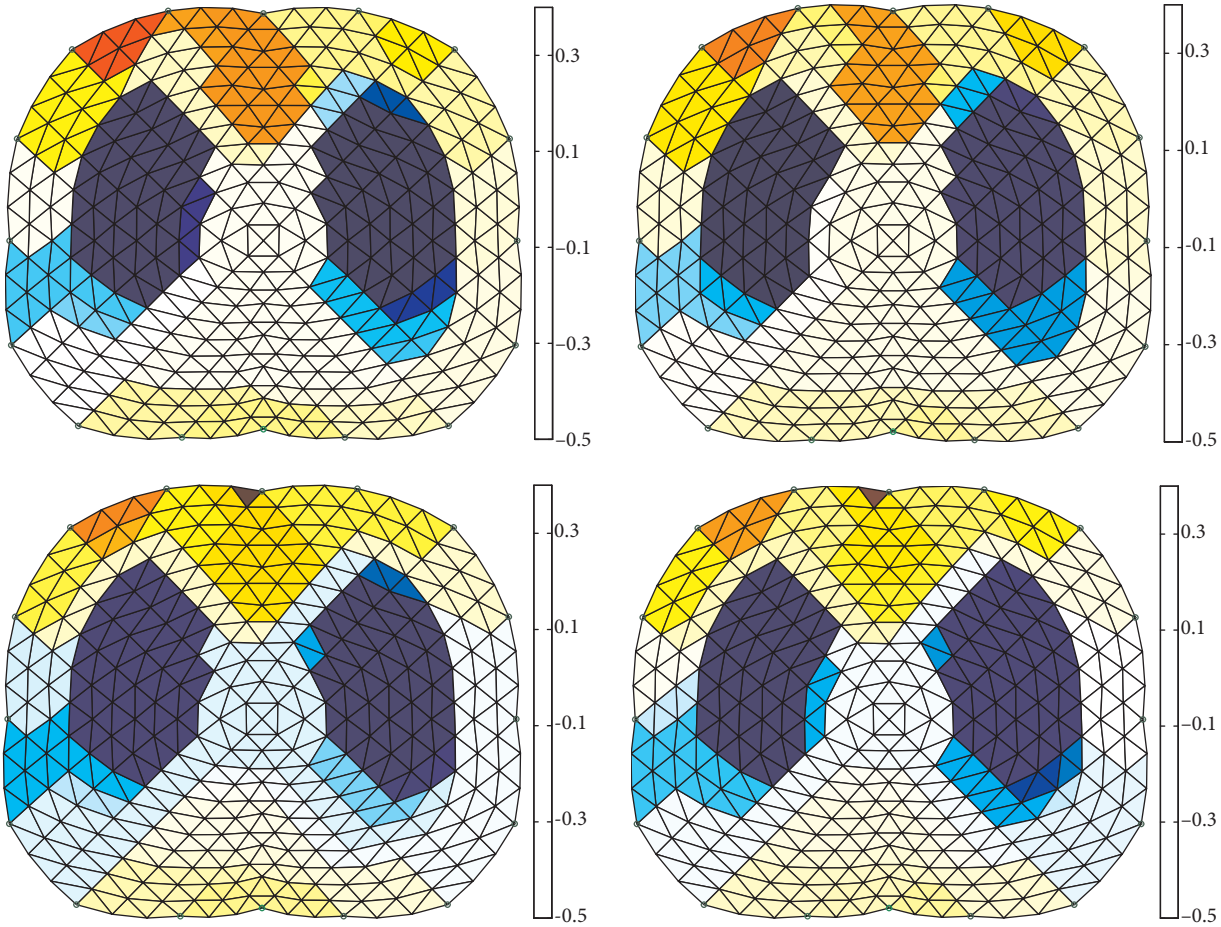

Figure 12. The conductivity change images reconstructed after the 12th iteration of the PD–IPM algorithm. The images have been reconstructed by the objective optimization, applying (a) 18th frame of the breathing cycle, (b) 22nd frame of the breathing cycle. The images have been reconstructed by the MRPM matrix, applying (c) 18th frame, (d) 22nd frame.

Table 4. The quantified values of the images of the 18th, 20th, and 22nd frames of the breathing cycle, obtained at the 12th iteration of the algorithm.

Number of frame	Objective optimization			MRPM optimization	
	α_T	CNR	COC	CNR	COC
Frame 18	1e–3	4.4987	7.829	5.391	8.430
Frame 20	1e–3	5.664	7.855	6.795	8.821
Frame 22	1e–3	4.579	7.728	5.474	8.357

4. Discussion

Although L^1 regularization schemes like the ones employing the total variation function encounter difficulties such as the non-differentiability of the absolute function in the neighborhood of zero, these techniques typically do not bias the solution toward the smoothest way, thus enabling detection of discontinuities over the domain [36,37].

The PD–IPM algorithm is the best-known TV regularized method applied in the context of EIT [16]. This algorithm can be run with much small values of β without imposing any difficulties for stability. The stability thus holds for a greater number of iterations in comparison with other algorithms such as lagged diffusivity [16]. The optimization of such a long iterative algorithm is thus an important challenge, and has been regarded in the EIDORS example entitled "Total Variation: choice of hyperparameters" [20].

The present study has initially optimized the standard algorithm via an objective method. The optimal regularization is the point that produces the image with the minimal RE among an extensive range of the regularization parameters when the RE values are plotted at the iteration where the convergence condition, i.e. Eq. (12), is satisfied. Other methods such as the fixed noise figure did not give the optimal solution since they could not adapt for the different levels of noise in the data. The values selected in the EIDORS website were far from the optimal point as well. Although the objective optimization is quite time-consuming, and is therefore not applicable for the lengthy iterative PD–IPM algorithm, it yields the most accurate solution that can be calculated from the standard algorithm. It is worth noting that the objective optimization is applicable merely in simulated studies, as the actual conductivity distribution is unknown in real cases. However, this study applied this method to in vivo measurements such that the images were approximately measured in terms of the parameters discussed in Section 3.4.2.

The algorithm was subsequently modified so that the scalar regularization parameter was replaced by a matrix derived from the square sensitivity matrix, according to Section 2.2. It was shown that the amounts of regularization required to reconstruct images of an impulse contrast moving from the center to the boundary of a circular model are not constant, but depend considerably on the normalized radial positioning of the impulse inclusion. This reflects the fact that the amount of regularization required over each region of the domain is contingent on sensitivity of the boundary measurements to that region. The information regarding the amount of regularization needed over various regions of the domain can be suitably extracted from the square sensitivity matrix.

The domain is thus divided into multiple subdomains so that the modified algorithm allocates different values for each of these subdomains. The value assigned to each subdomain is calculated as the mean of the square sensitivity matrix entries corresponding to that subdomain. The resulting matrix was termed multi-regularization parameter matrix (MRPM) here.

Applying the MRPM matrix rather than the scalar optimal regularization parameter surprisingly improved accuracy of the reconstructed images, as well as performance of the algorithm in detecting discontinuities over the images in both simulations and reality. In other words, the MRPM matrix directly produced images that are significantly sharper and more accurate than the images reconstructed by the objective optimization over a wide range of regularization parameters. Surprisingly, even after searching for the best choice of the scalar regularization parameter, the MRPM scheme has still outperformed the standard algorithm.

5. Conclusion

Indeed, fixing the amount of regularization applied to all finite elements prevents the reconstruction algorithm from adapting for different sensitivities of the boundary measurements to various regions of the domain. The performance of the MRPM scheme has even held for the data with a 10% noise level, equivalent to a SNR of 20 dB. This reflects the high capability of the applied scheme in reducing the condition number of the Hessian matrix, and as a result moderating the ill-posedness of the problem. Note that the objective selection of the regularization parameter is quite time-consuming due to the long iterative nature of the PD–IPM algorithm, becoming ineffective in application. Moreover, the objective optimization is not applicable in real situations

since the conductivity distributions of studied models are often unknown. However, this method was applied in order to make the most pessimistic comparison between the standard and the modified algorithms.

References

[1] A. Borsic, "Regularisation methods for imaging from electrical measurements". PhD thesis, Oxford Brooks University, 2002.

[2] C. Li, N. Duric, P. Littrup, L. Huang, "In vivo breast sound-speed imaging with ultrasound tomography", Ultrasound in Medicine & Biology Vol. 35, pp. 1625–1628, 2009.

[3] L.I. Rudin, S. Osher, E. Fatemi, "Nonlinear total variation based noise removal algorithms". Phys. D., Vol. 60, pp. 259–268, 1992.

[4] D.C. Dobson, F. Santosa, "Recovery of blocky images from noisy and blurred data". SIAM Journal on Applied Mathematics Vol. 56(4), pp.1181–1198, 1996.

[5] R. Acar, C.R. Vogel, "Analysis of bounded variation penalty methods for ill-posed problems". Inverse Problems, Vol. 10, pp. 1217–1229, 1994.

[6] D.C. Dobson, F. Santosa, "An image enhancement technique for electrical impedance tomography". Inverse Problems, Vol. 10, pp. 317–334, 1994.

[7] C.R. Vogel, M.E. Oman, "Iterative methods for total variation denoising". SIAM J. Sci. Computing, Vol. 17, pp. 227–238, 1996.

[8] T.F. Chan, H.M. Zhou, R.H. Chan, "A continuation method for total variation denoising problems". UCLA CAM Tech. Rep, pp. 95–18, 1995.

[9] T.F. Chan, G. Golub, P. Mulet, "A nonlinear primal dual method for TV-based image restoration". UCLA CAM Tech. Rep, pp. 95–43, 1996.

[10] C.R. Vogel, "Nonsmooth Regularization", in H.W. Engl, A.K. Louis, W. Rundell (Eds.), Inverse Problems in Geophysical Applications. SIAM Philadelphia, 1997.

[11] K.D. Andersen, "An efficient Newton barrier method for minimizing a sum of Euclidean norms". SIAM J. on Optimization, Vol. 6, pp. 74–95, 1996.

[12] K.D. Andersen, E. Christiansen, A. Conn, M.L. Overton, "An efficient primal-dual interior-point method for minimizing a sum of Euclidean norms". SIAM J. Sci. Comput., Vol. 22, pp. 243–262, 2000.

[13] S. Kim, K.M. Lustig, S. Boyd, "An interior-point method for large scale Ll-regularized least squares". IEEE Journal of Selected Topics in Signal Processing, Vol. 1(4), pp. 606–617, 2007.

[14] G. Shou, L. Xia, M. Jiang, "Total variation regularization in Electrocardiographic mapping". Lecture Notes in Computer Science, 6330 pp. 51–59, 2010.

[15] B.M. Graham, "Enhancements in electrical impedance tomography (EIT) image reconstruction for 3D lung imaging". PhD thesis, University of Ottawa, April 2007.

[16] A. Borsic, B.M. Graham, A. Adler, W.R.B. Lionheart, "In vivo impedance imaging with total variation regularization". IEEE Trans. Med. Imag., Vol. 29(1), pp. 44–54, 2010.

[17] S. Pan, X. Li, S. He, "An infeasible primal–dual interior point algorithm for linear programs based on logarithmic equivalent transformation", J. Math. Anal. Appl., Vol. 314, pp. 644–660, 2006.

[18] Y.Q. Bai, G.Q. Wang, C. Roos, "Primal_dual interior-point algorithms for second-order cone optimization based on kernel functions". Nonlinear Analysis, Vol. 70, pp. 3584–3602, 2009.

[19] G.Q. Wang, Y.Q. Bai, "Primal-dual interior-point algorithm for convex quadratic semi-definite optimization". Nonlinear Analysis, Vol. 71, pp. 3389–3402, 2009.

[20] EIDORS 3.5, Electrical Impedance Tomography and Diffuse Optical Tomography Reconstruction Software, 2011.

[21] http://eidors3d.sourceforge.net/tutorial/adv_image_reconst/TV_compare_hyperparams.shtml.

[22] A. Adler, R. Guardo, "Electrical impedance tomography: regularized imaging and contrast detection". Trans. Med. Imag., Vol. 15(2), pp. 170–179, 1996.

[23] B.M. Graham, A. Adler, "Objective selection of hyperparameter for EIT". Physiol. Meas., 27, pp. 65–79, 2006.

[24] J.L. Wheeler, W. Wang, M. Tang, "A comparison of methods for measurement of spatial resolution in two-dimensional circular EIT images". Physiol. Meas., Vol. 23, pp. 169–176, 2002.

[25] A. Adler, J.H. Arnold, R. Bayford, A. Borsic, B. Brown, P. Dixon, T.J.C. Faes, I. Frerichs, H. Gagnon, Y. Gaerber, B. Grychtol, G. Hahn, W.R.B. Lionheart, A. Malik, R.P. Patterson, J. Stocks, A. Tizzard, N. Weiler, G.K. Wolf, "GREIT: a unified approach to 2D linear EIT reconstruction of lung images". Physiol. Meas., Vol. 30, pp. 35–55, 2009.

[26] A. Javaherian, A. Movafeghi, R. Faghihi, E. Yahaghi, "Assessment of contrast positioning effects on reconstructed images of elliptical models in EIT applying different Current patterns". J. Applied Sci. Vol. 12(6), pp. 518–534, 2012.

[27] T.K. Bera, S.K. Biswas, K. Rajan, J. Nagaraju, "Improving conductivity image quality using block matrix-based multiple regularization (BMMR) technique in EIT : A simulation study". J. Electr. Bioimp., Vol. 2, pp. 33–47, 2011.

[28] A. Javaherian, A. Movafeghi, R. Faghihi, "Reducing negative effects of quadratic norm regularization on image reconstruction in electrical impedance tomography", Appl. Math. Model. (in press), available at: http://dx.doi.org/10.1016/j.apm.2012.11.022.

[29] EIDORS 3.5, Electrical Impedance Tomography and Diffuse Optical Tomography Reconstruction Software, 2011. http://eidors3d.sourceforge.net.

[30] EIDORS 3.5, Electrical Impedance Tomography and Diffuse Optical Tomography Reconstruction Software, 2011.

[31] http://eidors3d.sourceforge.net/tutorial/adv_image_reconst/total_variation.shtml.

[32] A. Boyle, A. Adler, "The impact of electrode area, contact impedance and boundary shape on EIT images". Physiol. Meas., Vol. 32, pp. 745–754, 2011.

[33] EIDORS 3.5, Electrical Impedance Tomography and Diffuse Optical Tomography Reconstruction Software, 2011.

[34] http://eidors3d.sourceforge.net/tutorial/EIDORS_basics/tutorial130.shtml.

[35] B.M. Graham, A. Adler, "Electrode placement configurations for 3D EIT". Physiol. Meas. Vol. 28, pp. 29–44, 2007.

[36] EIDORS 3.5, Electrical Impedance Tomography and Diffuse Optical Tomography Reconstruction Software, 2011.

[37] http://eidors3d.sourceforge.net/data_contrib/cg_deforming_tank_phantom/cg_deforming_tank_phantom_02.shtml.

[38] X. Song, B.W. Pogue, S. Jiang, M.M. Doyley, H. Dehghani, T.D. Tosteson, K.D. Paulsen, "Automated region detection based on the contrast-to-noise ratio in near-infrared tomography". Appl. Opt., Vol. 43, pp. 1053–1062, 2004.

[39] T.K. Bera, J. Nagaraju, "Resistivity imaging of a reconfigurable phantom with circular inhomogeneities in 2D electrical impedance tomography". J. Measurement., Vol. 44(3), pp. 518–526, 2011.

[40] B. Li, D. Que, "Medical images denoising based on total variation algorithm", Procedia Environmental Sciences Vol. 8, pp. 227–234, 2011.

[41] Y. Shi, X. Yang, "New total variation regularized $L1$ model for image restoration", Digital Signal Processing, Vol. 20, pp. 1656–1676, 2010.